Environmental Earth Sciences (2022) 81:188
https://doi.org/10.1007/s12665-022-10286-z

ORIGINAL ARTICLE

Novel iron-based nanocomposites for arsenic removal in groundwater: insights from their synthesis to implementation for real groundwater remediation

V. N. Scheverin[1] · A. Russo[2] · M. Grünhut[1] · M. F. Horst[1] · S. Jacobo[2] · V. L. Lassalle[1]

Received: 13 September 2020 / Accepted: 12 February 2022 / Published online: 16 March 2022

Abstract

The presence of arsenic in water samples of different nature represents a serious problem with severe consequences all around the world, but mainly in India, China, Central Africa, and Latin America. In this regard, the groundwater of the Bahía Blanca region (Bs. As. Province, Argentina in Latin America) clearly represents this problem, containing As levels higher than 200 μg L^{-1}. On many occasions, this resource is almost the unique source of water for human consumption and other uses. The available technology is not suitable and efficient enough to provide solutions in this context. This work proposes the preparation of low-cost, easy handle and efficient material to mitigate the As contamination problem. The aim is to provide useful materials that may be implemented in the real environment; in particular, to remediate groundwater from critical rural zone. Nanocomposites with different nominal ratios of zeolite and magnetite nanoparticles were synthesized. These materials were entirely characterized by FTIR, XRD, TEM, capillary microelectrophoresis, and dynamic light scattering. Adsorption assays were performed in batches using groundwater samples collected in the rural region of Bahía Blanca (southern Chaco-Pampean plain, Argentina). The stability and reuse capability of these adsorbents were evaluated. The possibility of designing a continuous flow system was also explored by comparing the As removal data achieved in this condition with the percentage of removal corresponding to the performed batch assays. The findings collected within this work appear very promising in view of the design of a household system to remove As from groundwater.

Keywords Magnetic nanocomposites · Zeolites · Arsenic removal · Groundwater

Introduction

Water availability for human consumption is considered a critical issue worldwide. Due to the increase in the world population, surface water resources are insufficient to meet the demand (Nordstrom 2002). This situation may be solved by employing alternative natural water sources, such as groundwater. However, although it could be an excellent option to ensure water demand, it can present a severe disadvantage related to its high content of potentially harmful compounds, including arsenic (As) (Chen et al. 2017; Merola et al. 2014; Rango et al. 2013).

Arsenic pollution of groundwater is considered a major public health problem globally due to its carcinogenic and neurotoxic properties. Consumption of water naturally contaminated by arsenic does not result in acute intoxication. However, serious health effects have been reported in populations drinking arsenic-rich water for prolonged periods of time. Chronic arsenic intake is associated with the appearance of arsenicosis, known in Latin America as chronic regional endemic hydroarsenism (HACRE), characterized by presenting severe skin lesions and cancerous and non-cancerous systemic alterations.

Reported data suggest that millions of people in the world are exposed to higher As concentrations than those recommended by World Health Organization (WHO) for drinking water (10 μg L^{-1}) (Nordstrom 2002; World Health

✉ V. L. Lassalle
veronica.lassalle@uns.edu.ar

[1] Instituto de Química del Sur (INQUISUR), Departamento de Química, Universidad Nacional del Sur, CONICET, Bahía Blanca, Argentina

[2] División Química de Materiales Magnéticos de Aplicación a La Ingeniería (DiQuiMMAI), Facultad de Ingeniería, UBA INTECIN-CONICET, Buenos Aires, Argentina

Organization 2011). The most affected regions are India, China, Central Africa, and Latin America (World Health Organization 2011). In Latin America, at least 14 countries are affected by this problem, with the most critical zones located in Chile, México, and Argentina (Bundschuh et al. 2012; Litter et al. 2010). Particularly in Argentina, the number of people exposed to As concentration higher than 10 µg L^{-1} reaches almost 4 million, representing about 10% of the total actual country population. It is important to highlight that most of them correspond to rural population (Bundschuh et al. 2008). One of the most affected areas is the Chaco-Pampean plain, which is one of the largest regions in the world of high arsenic groundwater (Smedley and Kinniburgh 2002), reaching Arsenic concentration up to 5000 µg L^{-1} (Smedley et al. 2002). Notably, in Bahía Blanca, a city located in southern Chaco-Pampean plain, the groundwater used for human consumption and irrigation presents, in some cases, high levels of arsenic in groundwater. Arsenic levels on the order 10–300 µg L^{-1} depending on the screened zone have been reported in this area (Al Rawahi 2016; Blanco et al. 2006; Gomez et al. 2009; Paoloni et al. 2009; Villaamil Lepori 2015).

Despite the efforts of the academic and industrial sectors, the problem related to arsenic removal from groundwater persists. Reaching allowed arsenic concentration levels continues to be a challenge of great interest that has become part of the public agenda in many countries. The water matrix composition is a critical aspect for efficient in this concern (Yan et al. 2012). Physicochemical characteristics of the matrix will determine the most convenient technology for efficient As removal. The economic factor is also an important parameter to take into account with regards to the technology selection, especially in rural areas where economic resources are usually limited.

Several procedures have been explored, including membrane process, ion exchange, coagulation, and adsorption (Garelick et al. 2005; Hao et al. 2018). Among these tools, membrane and ion-exchange processes are hardly implemented in rural zones due to their expensive installation and maintenance costs, while chemical precipitation results in the toxic sludge formation with high pollutant content (Habuda-Stanić et al. 2014). Therefore, arsenic concentration below 10 µg L^{-1} is usually difficult to attain (Hao et al. 2018). In this sense, adsorption appears as one of the most promising strategies due to their cost/efficiency ratio, which involves potential reuse and possible applications at community/household levels (Garelick et al. 2005).

Due to its high efficiency, the use of iron-based adsorbents for arsenic removal has been extensively reported in the literature. In this context, nanoscale zero-valent iron (nZVI) and magnetite nanoparticles (M) are two of the most commonly reported adsorbents (Garelick et al. 2005; Hao et al. 2018; Lata et al. 2016). However, the application of these materials is limited because of stability issues regarding iron leaching, which leads to an additional component in the water to be remediated (Ai et al. 2011; Hao et al. 2018; Inbaraj et al. 2011; Liu et al. 2008; Matei et al. 2011). The loading of nZVI or M onto appropriate supporting materials may partially overcome this limitation, avoiding undesirable iron leaching into the water (Hao et al. 2018). A great diversity of compounds can be employed as support for the design of iron-based adsorbents, including natural and synthetic polymers, clays, etc. (Popescu et al. 2019). Among them, particular interest has arisen regarding the use of natural zeolites (Abdullah et al. 2019).

The zeolites are framework silicates consisting mainly of interconnecting tetrahedrons of SiO_4 and AlO_4. The requirement to be considered a zeolite is that the ratio Si + Al/O must be ½. In this way, the aluminosilicate structure becomes negatively charged and attracts the positive cations residing within it. Among aluminosilicate compounds, zeolites are recognized as promising hosts and stabilizers owing to their exceptional properties such as high ion-exchange capacity, large surface area, hydrophilicity, eco-friendly nature, easily tunable chemical properties, and high thermal stability (Alswata et al. 2017).

In the most used zeolites, the spaces are interconnected and form long wide channels of varying sizes depending on the mineral. These channels allow the easy movement of the resident ions and molecules into and out of the structure, conferring zeolites improved adsorbent properties, including against inorganic pollutants such as heavy metals or arsenic (Kanel et al. 2005, 2006; Zhangtao Li et al. 2018; Salem Attia et al. 2014; Suazo-Hernández et al. 2019; Václavíková et al. 2009).

The formation of composite hybrid materials from the combination of magnetite and zeolite has been extensively reported (Abdullah et al. 2019). This type of materials has been applied in diverse fields, being water remediation one of the most explored (Abdullah et al. 2019; Kharissova et al. 2015). For instance, Yuan et al. assessed the adsorption capacity of magnetite–zeolite composites to remove Pb^{2+} from model solutions. They used an adsorbent dosage of 0.2 mg mL^{-1}, an initial concentration of 71.9 mg L^{-1} $Pb(NO_3)_2$ solution at a temperature of 25 °C, and a contact time of 2 h (Yuan et al. 2011). Another group of pollutants removable by magnetic–zeolite composites is the dyes. The use of magnetite–zeolite nanocomposites to eliminate malachite green dye from an aqueous solution has been reported (Jain et al. 2015).

The results informed by the authors reveal a high adsorption capacity mediated by a spontaneous and exothermic process. The authors identified the role of each component of the nanocomposite. They suggested that the zeolite provides suitable adsorption properties as well as prevents aggregation of the iron oxide nanoparticles, contributing to

their storage and palletization; whereas, the magnetic component contributes to the magnetic affinity, providing the adsorbent with the possibility of being simply removed from the remediation medium by exposure to a magnet.

Adsorption of arsenic by iron-based zeolite composites has also been reported (Hao et al. 2018). The work of Pizarro et al. shows that nanomagnetic zeolite, sized of about 50 nm, functioned as an efficient adsorbent for the removal of arsenic (Pizarro et al. 2015).

From this brief survey, it is clear that, although a great volume of available literature may be found referring to the synthesis and application of zeolite–magnetite composites for water remediation, most of the information is devoted to basic studies involving mainly model aqueous solutions containing selected pollutants. Therefore, scarce data are found related to the efficiency and performance of such materials applied to real water matrix, such as groundwater (Hao et al. 2018; Lata et al. 2016; Suazo-Hernández et al. 2019; Tanboonchuy et al. 2012).

This work aims to synthesize, characterize, and apply iron-based zeolite composites as adsorbent materials destined for arsenic removal from groundwater. This focus includes the analysis of physicochemical properties of prepared composites as well as the raw materials (iron oxide and zeolites) and the evaluation of their performance in eliminating As from groundwater. For this purpose, a sample of real groundwater, with complex matrix and high arsenic content (almost 200 µg/L), from the southern of the Buenos Aires Province (Argentina) has been employed. In this way, it is intended to provide a more realistic perspective in terms of the efficiency of the proposed materials for arsenic removal from groundwater. This contribution also includes the implementation of continuous flow system at lab scale as a proposal for the practical application of the adsorbents proposed within this work. This feature may be considered as a first approximation to a groundwater remediation system at household scale.

Experimental

Materials

The natural zeolite (Z) used in this work was supplied by DIATEC S.R.L., and extracted from La Rioja deposit (Argentina). For the synthesis of magnetite–zeolite composites, Z was previously ground and sieved to obtain 297 µm particle size. All used reagents were of analytical grade. Ferric chloride hexahydrate (99.99%) was provided by Biopack (Argentina), ferrous sulphate heptahydrate (99.99%) was provided by Mallinckradt Chemical Works (USA), and sodium hydroxide was purchased from Cicarelli (Argentina).

Methods

Synthesis of zeolites-Fe (ZFe)

The Z loaded with zero-valent iron was synthesized by an ion-exchange procedure followed by a reduction process according to a methodology previously reported (Russo et al. 2014). Briefly, 32 g of Z were immersed in an aqueous solution of $FeSO_4$ (0,14 M) for 24 h. After the exchange procedure, the sample was purified with double-distilled water. Then, Fe (II) reduction was carried out by adding KBH_4 solution to an aqueous dispersion of the sample in a nitrogen atmosphere. The solid obtained was ground and sieved to obtain a particle size of 297 µm.

Synthesis of magnetite nanoparticles (M)

The synthesis of M was carried out by the co-precipitation method employing conditions previously studied in the research group (Azcona et al. 2016; Lassalle et al. 2011). Briefly, 100 mL of a ferric and ferrous solution (2/1 molar ratio) was prepared and stirred for 30 min under N_2 bubbling. Then, 25 mL of NaOH 5 M solution were added at a controlled rate (approximately 1 mL min^{-1}), to obtain magnetite at the nanoscale. The black precipitate formed was isolated using a magnet and washed several times with double-distilled water until the supernatant showed conductivity values similar to those presented by the double-distilled water. The solid was dried at 40 °C for 24 h.

Synthesis of magnetite–zeolite nanocomposites (MZ)

MZ nanocomposites were synthesized using an adaptation of the chemical co-precipitation method of magnetic nanoparticles on zeolite moieties (María F. Horst et al. 2016). In brief, 1.00 g of Z was added to a prefixed volume of ferric/ferrous solution with a molar ratio of 2/1. The suspension was stirred at 70 °C for 30 min under N_2 bubbling. The subsequent procedure was the same as described for the synthesis of magnetite nanoparticles (Sect. 2.2.2). Two formulations were prepared by modifying the M/Z mass ratio as follows: MZ (1:1) and MZ4 (1:4).

Characterization

The composition of the materials was estimated in terms of iron content by atomic absorption spectroscopy (GBC Avanta 932 Spectrometer). An adequate amount of sample was disaggregated with an acid solution (10% HCl) for analysis.

The FTIR spectra were recorded on Thermo Scientific Nicolet iS50 over the range 4000- compressed into a pellet.

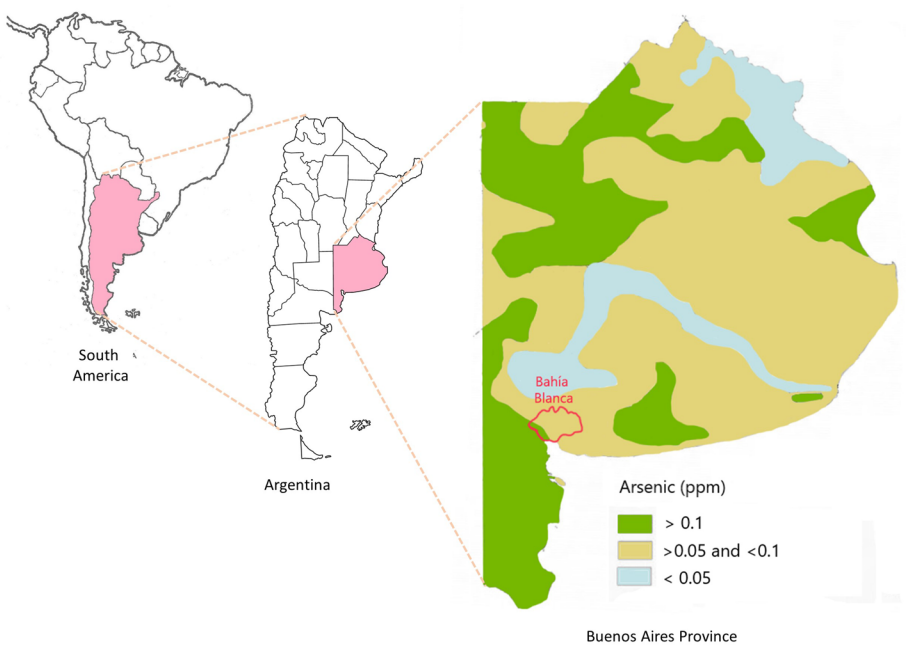

Fig. 1 Geographical location of Bahía Blanca city and the distribution of As in the groundwater of the Buenos Aires Province

X-ray diffraction (XRD) analyses were performed by a PANalytical Empyrean 3 diffractometer with Ni-filtered CuKα radiation, a graphite monochromator, and a PIXcel3D detector. It was operated at a voltage of 45 kV and a current of 40 mA, in the 2Θ range from 5° to 70° using a continuous scan mode with a scan angular speed of 0.016° min^{-1}. An estimation of the crystallite size of magnetite nanoparticles has been performed from the Scherrer equation

$$D = \frac{K\lambda}{\beta \cos\theta},$$

where D is the crystal size (nm), K is the shape factor, λ is the X-ray wavelength (nm), β is the full width at half-maximum (FWHM) of the strongest peak of magnetite (3 3 1), and θ is the Bragg's angle.

Zeta potential (ξ) and hydrodynamic diameter (HD) were measured with a Malvern Zetasizer Nano ZS90. For ξ measurements, samples containing 5 mg mL^{-1} of material in 0.01 M NaCl were prepared, and the pH was adjusted in the range between 9 and 4 with 0.01 M NaOH or HCl solutions. On the other hand, for HD determinations, aqueous dispersions (0.1 mg mL^{-1}) of the composites and raw materials were prepared using filtered double-distilled water at pH 6. All dispersions were sonicated for 30 min prior to the assay. In all cases, the dispersions displayed a unimodal diameter distribution.

Morphology was examined by transmission electron microscopy (TEM) using a JEOL 100 CX II, (JEOL, Tokyo, Japan 1983) microscopy. The samples were dispersed in distilled water/ethanol, placed on 200 mesh Cu grids, and dried at room temperature.

Adsorption assays

Characteristics of the real groundwater

The groundwater sample employed in the adsorption assays was collected in the southern Chaco-Pampean plain of Argentina in Bahía Blanca district, south of Buenos Aires province. Figure 1 shows the distribution of As in groundwater of Buenos Aires Province (Auge et al. 2013). In particular, the sample was collected from a rural school environment where the shallow groundwater is the only water source and exhibits high As concentration, reaching almost 200 μg L^{-1} in certain periods of the year. The coordinates of the sample point are Latitude 38°35′42.6" S and Longitude 62°23′12.1" W of Greenwich.

The sample groundwater was extracted by windmills and collected in sterile containers. Its analysis regarding composition is shown in Table 1. For the experiments, the pH was not regulated and the sample was not filtered.

Adsorption assays

The adsorption performance of the prepared materials in As removal from the groundwater sample described in the section "Characteristics of the real groundwater", was evaluated as a function of time. To this end, a series of batch experiments were performed by employing an adsorbent mass: volume of sample ratio of 3:1. Different batches were prepared and the water sample was treated during 15, 30, 60, 120, 180, and 360 min, respectively, at room temperature. In the case of ZMs, they were separated from the supernatant by magnetic decantation for 5 min, while the materials

Table 1 Chemical composition of shallow groundwater used for real water adsorption

Parameter	Value	Unit
As	201	μg L^{-1}
F^-	14.40	mg L^{-1}
Na	626	mg L^{-1}
SO_4^{2-}	542	mg L^{-1}
Cl	260	mg L^{-1}
pH	8.70	
Electrical conductivity	4.38	mS/cm

minicolumn packed with 60 mg of MZ (Fig. 2). The minicolumn was made using a Tygon® tube (length: 45 mm; inner diameter: 3 mm). The sample was pumped with a Gilson model Minipuls 3 peristaltic pump. All the flow system components were made of PTFE (0.5 mm i.d.).

For the flow assay, 20 mL of the sample were pumped towards the minicolumn at a flow rate of 0.20 mL min^{-1}. The sample treated was collected in a flask placed at the end of the line. It is important to highlight that the ratio adsorbent mass/volume of water remained constant about batch assays (i.e., 3:1). The procedure was performed at room temperature.

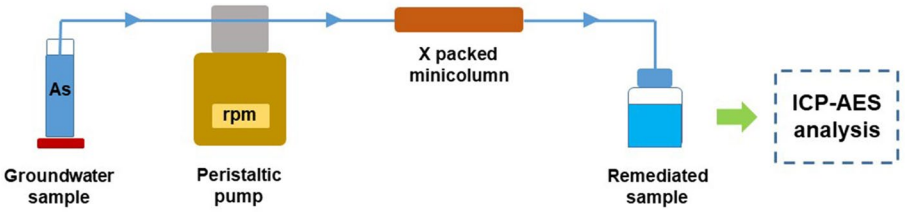

Fig. 2 Scheme of the continuous flow system used for on line arsenic adsorption in groundwater samples. The rows indicate the direction of the flow

without magnetic properties were separated by centrifugation at 6000 rpm for 8 min.

Total arsenic concentration was quantified in the supernatants by atomic emission spectroscopy (ICP-AES Shimadzu 1000 mod III) with a quantification limit of 10 μg L^{-1}. All the samples were filtered and frozen until their measurement. The percentage of As removed was calculated from the following equation:

$$\%R = \frac{(C_i - C_f) \times 100}{C_i},$$

where C_i and C_f are the initial and final concentration of As in the supernatant of adsorption, expressed in μg L^{-1}, respectively.

Reusability assays

The reusability of magnetic materials in the groundwater sample was studied over 4 consecutive cycles, at a fixed time. For these experiments, the same mass adsorbent–volume of sample ratio was used as in the section "Adsorption assays", without any purification/regeneration step between cycles.

Flow assays

The performance of selected adsorbents was also evaluated in a lab-scale continuous flow system in a way to simulate almost operative conditions after the implementation as a real remediation system. Such a system included a

On the other hand, reuse adsorption assays were carried out using the continuous flow method. A total of four cycles were performed using fresh real water samples in each cycle.

Results and discussion

Characterization of adsorbent materials

Figure 3 illustrates the structure of the prepared materials. As can be observed in the images, the magnetic composites are easily attracted by a magnet. Thus, they may be removed from the aqueous media by exposure to an external magnetic field. It is worth noting that the differences concerning their composition and the chemical interactions between the different components lead to materials with significant differences concerning their adsorption capability and stability in the application medium, as will be described in the different sections all over the work.

Composition

The composition of Z, ZFe, M, MZ, and MZ4, in terms of the Fe contents, is listed in Table 2. For the magnetic composites, the fraction of the iron-based phase was estimated considering that all iron content comes from magnetite (Fe_3O_4). In the case of M, a percentage of Fe_3O_4 lower than 100% was registered. This result may be ascribed to the formation of other Fe oxides different from the magnetite, as minority phase. In fact, goethite (α-FeOOH) and maghemite

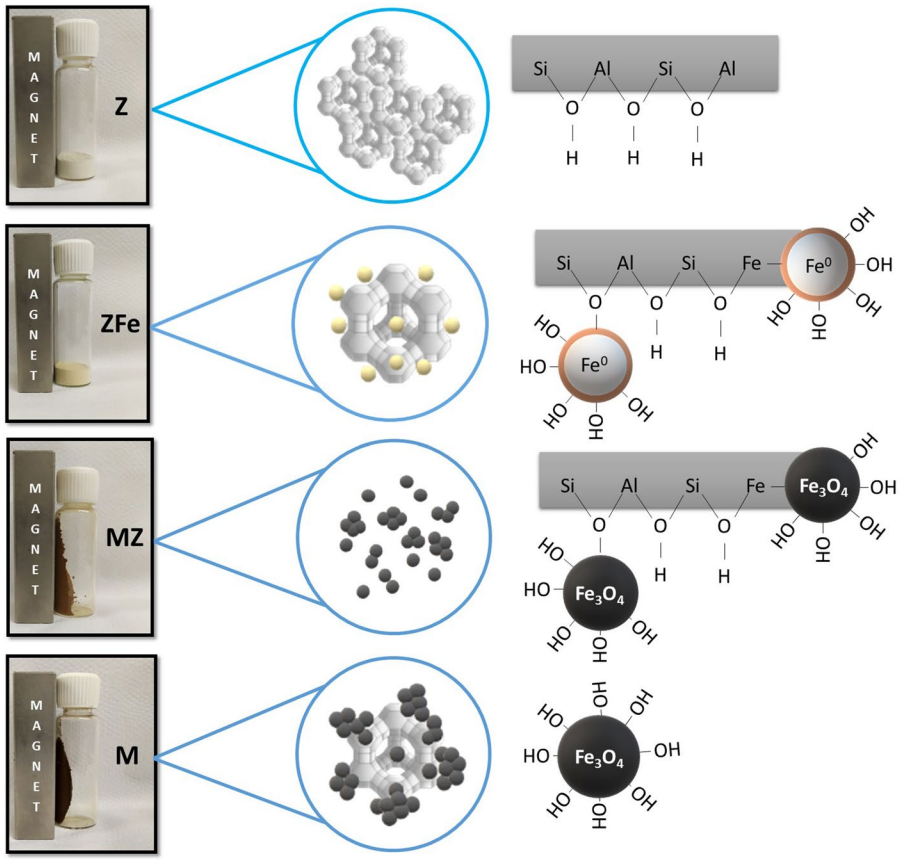

Fig. 3 Schematic representation of chemical structure of adsorbents prepared within this work

Table 2 Composition of prepared materials expressed as iron content and magnetic phase

Sample	g Fe/g_m	Fe_3O_4 g/g_m	% Magnetic phase	% Zeolites
Z	0.014	–	0	0
ZFe	0.021	–	0	0
M	0.616	0.852	85.2	0
MZ	0.380	0.526	52.6	47.4
MZ4	0.182	0.252	25.2	74.8

(Υ-Fe_2O_3) are the most commonly reported impurities found during magnetite synthesis by the co-precipitation method. The formation of these impurities could be related to the partial oxidation of Fe^{2+} ions to Fe^{3+}. Thus, effective Fe^{3+}/Fe^{2+} ratio increases concerning the initial ratio of 2:1 (Maity et al. 2007). Some reports, such as the one corresponding to Gnanaprakash et al. indicated that the use of strong alkaline media could cause the formation of non-magnetic iron compounds (Gnanaprakash et al. 2007).

The data obtained for MZ and MZ4 show that the % of magnetic phase determined by the Fe content perfectly coincides with the nominal proportions feed to the reaction. These results suggest that the presence of zeolite in a co-precipitation medium would favor the formation of magnetite over other oxides.

X-ray diffraction

The XRD diffractograms of Z and ZFe have been previously studied in another work (Russo et al. 2014). Analysis of the experimental data indicates that the crystalline pattern of Z mainly agrees with that corresponding to clinoptilolite. On the other hand, the diffraction pattern of ZFe does not show significant differences regarding Z. This implies that the crystalline structure of clinoptilolite was retained after modification (data not shown; included in (Russo et al. 2014)). In addition to the characteristic peaks of clinoptilolite, other peaks of lower intensity were found. Some of them may be identified as aluminum and sodium oxides, which are the main compositional elements of zeolite (Wang et al. 2010).

Figure 4 shows the diffractograms of samples M, MZ, and MZ4, and includes the patterns of magnetite (JCPDS 19–0629) and clinoptilolite (JCPDS 39–1383) for comparison. It is important to highlight that magnetite and maghemite cannot be distinguished by XRD, because they share the same spinel structure and almost identical lattice parameters (Darminto et al. 2011; Kim et al. 2012). In the diffractogram of M, peaks at $2\Theta = 18.2$ (1 1 1), 30.2 (2 0 0), 35.5 (3

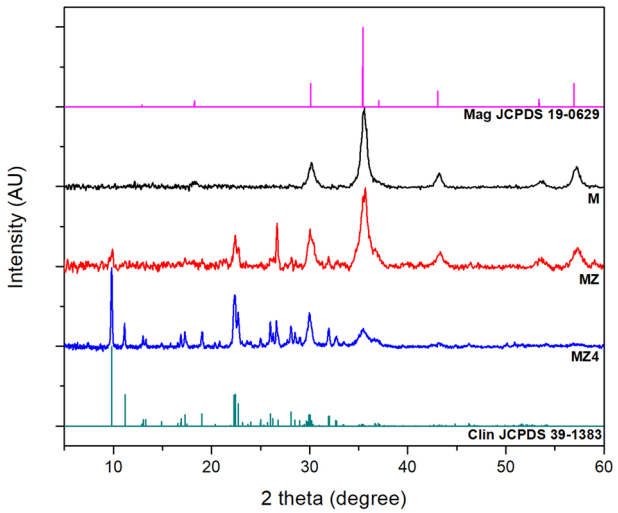

Fig. 4 XRD difractograms of the prepared composites

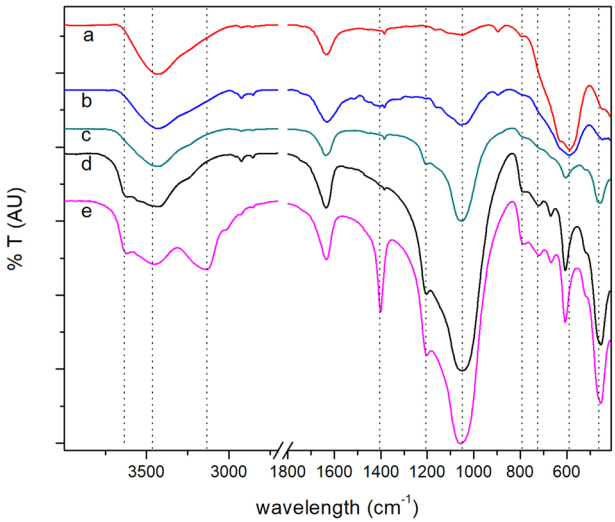

Fig. 5 FTIR spectra of a) M, b) MZ, c) MZ4, d) Z, and e) ZFe

1 1), 43.2 (4 0 0), 53.7 (4 2 2), and 57.3 (5 1 1) allow verifying the presence of magnetite, and eventually maghemite.

The XRD diffractograms corresponding to MZ and MZ4 composites present the characteristic peaks of magnetite and clinoptilolite, revealing that not notable changes occurred in positions of the relevant reflections concerning standard patterns. These findings indicate that the composites retain the crystalline structure of M and Z.

A reduction in the crystallinity is noted by increasing zeolite proportions. This behavior may be ascribed to changes in the laminar structure of the zeolite. Information in the open literature depicts that incorporation of iron-based moieties, such as $Fe(OH)/Fe_3O_4$, leads to an expansion in the unit cell dimension, possibly due to the isomorphic substitution of trivalent iron for the tetravalent aluminum in the framework (Bosînceanu et al. 2008; Rahmani et al. 2015).

The crystallite sizes for M, MZ, and MZ4, calculated by the Scherrer equation, were 15.8, 15.8, and 10.64 nm, respectively. This trend suggests that increasing the Z proportion hindered the possibility of magnetic particles to grow. This trend has been observed in other works were zeolites and clays, and even polymeric moieties have been used in the co-precipitation environment of magnetite nanoparticles (Singh et al. 2016).

FTIR spectroscopy

Figure 5 shows the FTIR spectra recorded for all adsorbent materials. The Z spectrum exhibits the most intense bands in the range of 1200–900 cm^{-1}, associated with the internal vibration of Si–O-X (X = Al; Si). Signals related to internal X–O-bond linkages in XO_4 of zeolite lattices appear in the range of 900-400 cm^{-1}, while signals ascribed to OH-bridging groups are visualized near 3600–1600 cm^{-1} (Blanco Varela et al. 2006).

The M spectrum confirms the presence of magnetite, although the presence of traces of other iron oxides (goethite, maghemite) as impurities may not be discarded. For instance, the splitting of the band centered at 590 cm^{-1}, corresponding to the vibrations of Fe–O bonds, likely indicates the presence of maghemite. According to the literature reports (Bruce et al. 2004), when this band is not symmetrical or eventually splits it can be considered evidence of the presence of maghemite. On the other hand, the presence of goethite is evidenced by the characteristics bands at 895 and 792 cm^{-1}, in agree with available literature (Nasrazadani et al. 1993; Stoia et al. 2016).

The spectra of MZ and MZ4 nanocomposites evidence significant changes compared to those corresponding to Z. The shifting and deformation of peaks related to the stretching vibration of Si–O–Si (1200 cm^{-1}) and Si–O–Al (1048 cm^{-1}) may be attributed to changes in Si–O–Si bonds and partial elution of Al^{3+} during the synthesis process, respectively (Korkuna et al. 2006; Rahmani et al. 2015). These changes suggest that a partial Al^{3+} replacement occurred during the synthesis procedure of magnetite–zeolite composites. These findings are in agreement with those arising from XRD analysis. Further evidence of Fe–Si interactions can be found in the shift of the band located at 792 cm^{-1} related to SiO_4 (Arruebo et al. 2006; Blanco Varela et al. 2006).

On the other hand, the spectra of both nanocomposites show the absence of the band associated with bridging O–H groups in ≡Si–OH-Al≡ (3616 cm^{-1}). The disappearance of this band for magnetic nanocomposites indicates that these specific O–H bonds are involved in the Fe–Z interactions

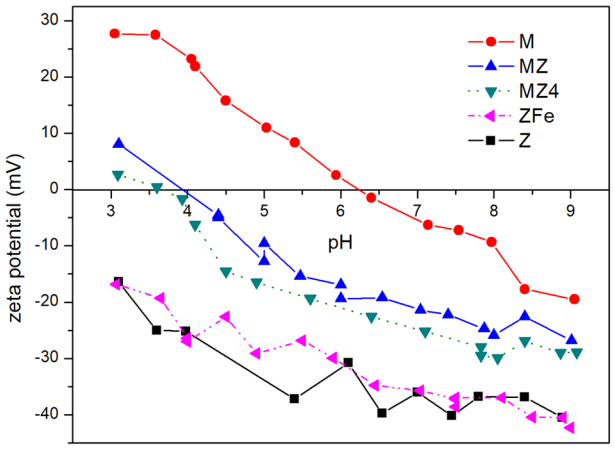

Fig. 6 Evolution of Z potential as a function of the pH for the studied solids

(Doula 2007). Thus, it could be inferred that interaction between the OH structural groups of zeolite and Fe_3O_4 nanoparticles is mainly responsible for the magnetic nanoparticles linkage on the zeolite moieties (Olad et al. 2010).

The spectrum of the MZ nanocomposite exhibits the bands related to the iron oxide component. The band located at 589 cm^{-1} entirely overlaps with those associated with X–O bonds located at frequencies lower than 800 cm^{-1}. Conversely, in the spectrum of the MZ4 nanocomposite, the band particularly associated with Fe–O bond is not detected, but only a widening of the signals below 800 cm^{-1} respect to Z spectrum is noticeable. Other authors reported similar results synthesizing similar materials under comparable conditions (Mthombeni et al. 2016; Yamaura et al. 2013).

The FTIR spectrum of ZFe does not show significant differences regarding Z spectrum in terms of the position of the characteristic zeolitic bands. The signals associated with Si–O–X vibration appear at the same position in both materials (1048 cm^{-1}). Thus, it could be inferred that the replacement of Al^{3+} during the ZFe synthesis procedure was limited (Doula 2007). On the other hand, in ZFe spectrum, the band associated with the vibration of bridging O–H groups in ≡Si–OH-Al≡ (3616 cm^{-1}) remains unaltered. Besides, the sharp peaks around 3180 y 1400 cm^{-1} may be related to the presence of N–H groups arising from the ammonia treatment in the synthesis procedure (Bakatula et al. 2015).

Zeta potential measurements

Figure 6 shows the evolution of ζ as a function of pH for all materials. It is evident that Z and ZFe materials develop a negative ζ along the entire pH range; hence, no isoelectric point (IEP) is found. The IEP of M was 6.32, in good agreement with the value reported by other authors for magnetite (Kosmulski 2016; Sun et al. 1998). The presence of other iron oxide phases would cause a shift in the IEP (Parks 1967). Then, this study did not evidence the presence of a significant amount of impurities (goethite and maghemite).

Conversely, both magnetic nanocomposites exhibit different behavior concerning their precursors, which may be considered additional evidence of the formation of distinct compounds with specific properties, as suggested by other authors working with similar Z-based nanosystems (Suazo-Hernández et al. 2019).

MZ and MZ4 show IEP at values of pH of 4.1 and 3.72, respectively. Although both materials show a similar pH dependence profile, ζ values for MZ4 are lower than those registered for MZ over the whole pH range. These results agree with the findings of other authors, suggesting that the values of ζ and IEP are directly related to the composition of a binary system (Gil-Llambias et al. 1982; Parks 1967).

The magnitude of the ζ is commonly employed as a criterion to estimate the colloidal stability of a nanoparticulated dispersion. It is important to remark that MZ materials exhibit suitable colloidal stability at pH 8–9, which is the typical range for shallow groundwater of the sampled area (Auge et al. 2013).

Table 3 Hydrodynamic diameter and polydispersity index of all materials dispersed in bi-distilled water

Material	HD ± σ (nm)	PDI
M	302.6 ± 8.8	0.3423
MZ	384.0 ± 4.1	0.4100
MZ4	383.6 ± 9.9	0.2430
ZFe	736.8 ± 42	0.6710
Z	1115.2 ± 259	0.9773

Size and morphology

Table 3 shows the size of the raw and composite materials in terms of average hydrodynamic diameter (HD) and polydispersity index (PDI). The high HD and PDI values for Z and ZFe may be ascribed to the grinding and sieving process implemented in obtaining the materials. This process may lead to particles with a wide range of size and significant size heterogeneity (Arruebo et al. 2006).

The HD for M, MZ, and MZ4 appear within the same range, i.e., all about 300–400 nm, with acceptable PDI values. Instead, the HD registered for both composites materials are lower concerning the HD values reordered for raw Z. In relation to this, Burris et al. reported a considerable size reduction of natural zeolites after acid treatment (Burris et al. 2016). In this sense, during the synthetic procedure of the nanocomposites, before adding NaOH, the co-precipitation medium is highly acidic (pH almost 1.5–2). Hence, the reduction of hydrodynamic diameter of composites

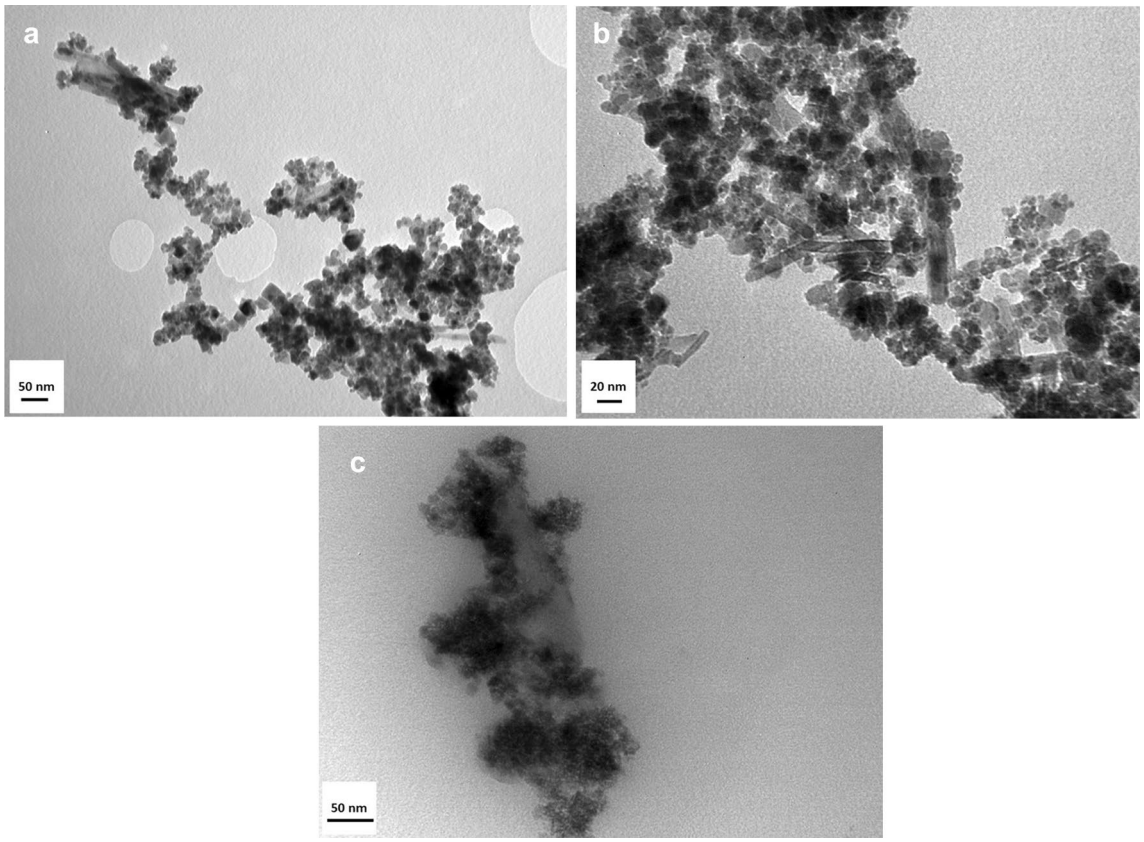

Fig. 7 TEM micrographs of **a** M, **b** MZ, and **c** MZ4 samples

materials, compared with HD of Z, may be associated with the conditions. Moreover, the nucleation and growth mechanism followed by magnetite nanoparticles in the formation contribute to reducing Z aggregation by inducting the growth around the magnetic core (Fernanda Horst et al. 2017; Nicolás et al. 2013).

TEM micrographs of magnetic materials M, MZ, and MZ4 are included in Fig. 7. The images reveal the presence of a crystalline phase, mainly of octahedral morphology, with a non-homogeneous distribution. In concordance with the observed by XRD and FTIR, the presence of nano-rods could be associated with the presence of goethite as an impurity (Mohammed et al. 2017).

For MZ and MZ4, the observed morphologies are compatible with the occurrence of Fe_3O_4 nanoparticle agglomeration onto the zeolite frameworks. Besides, the aggregation of surface particles decreases with increasing zeolite content in composite materials (Singh et al. 2016). Such aggregation may be induced by the small size of the magnetic core (on the order of 10–30 nm) and the high dipole–dipole and magnetic interactions. This behavior is typical when magnetite nanoparticles are immobilized in porous supports (Abdullah et al. 2017; Singh et al. 2016).

Adsorption assays

The adsorption performance of the materials was tested by analyzing their ability to retain total As from groundwater collected in the rural area of Bahía Blanca (Chaco-Pampean plain, Buenos Aires, Argentina). At sample pH, As^{3+} is mainly present as neutral H_3AsO_3, while the dominant species of As^{5+} are $H_2AsO_4^-$ and $HAsO_4^{2-}$ (Hao et al. 2018).

The adsorption process is strongly dependent on the contact time. Rapid adsorption kinetics means less residence time. Therefore, in terms of cost-effectiveness, the maximum removal of the contaminant in the shortest possible time is desired. Figure 8a shows the adsorption efficiency (expressed as % As removed) of the prepared materials as a function of the time. It is worth noting that raw Z was not efficient for As removal in the time selected to achieve the adsorption assays (data not shown). This behavior could be explained in terms of insufficient contact time and the physicochemical properties of Z. In this regard, other authors have reported similar results for untreated clinoptilolite-type zeolites. Li et al. (2007) informed that natural clinoptilolite showed no affinity for As(V) even after 24 h of assay. Besides, Elizalde-Gonzalez et al. (2001) reported that after

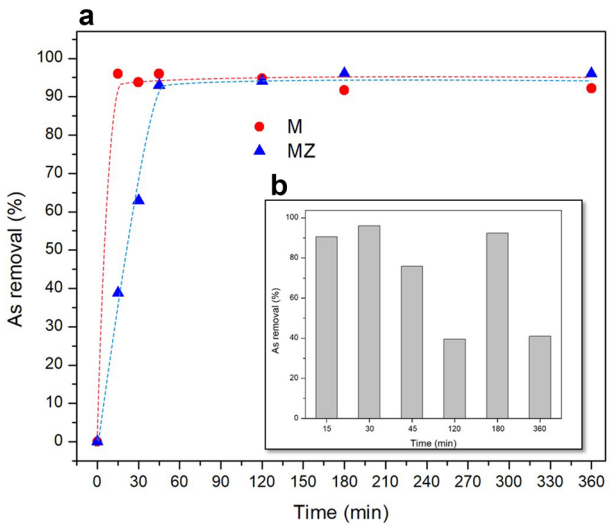

Fig. 8 **a** Adsorption profile of M and MZ expressed as % As removal vs. time; **b** adsorption profile of ZFe

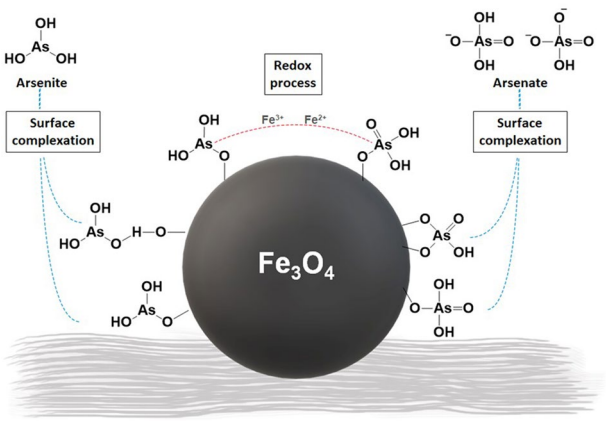

Fig. 9 Schematic representation of the feasible mechanism involved in the adsorption of As^{3+} and As^{5+} onto iron oxide-based composites

the acidic activation of natural clinoptilolite, an improvement in the efficiency of arsenate removal, from 15 to 90%, after 7 days of contact, was achieved using a water sample comparable to the one employed within this work.

The As adsorption capability of ZFe appears to be fluctuating against the time, as shown in Fig. 8b. This suggests that, despite the initial rapid removal, the system did not reach the equilibrium during the time fixed for the assay. This behavior could be explained by taking into account the presence of multiple additional unknown species presents specifically in the groundwater sample used. The presence of co-existing ions, such as NO_3^-, PO_4^{3-}, SO_4^{2-}, and HCO^{3-} might compete with As for adsorption sites on ZFe (Bhowmick et al. 2014; Kanel et al. 2005, 2006; Suazo-Hernández et al. 2019). Besides, the pH value of sample water could cause leaching of iron from the adsorbent. In this sense, Dorathi and Kandasamy (2012) informed significant iron leaching on nZVI impregnated into silica at pH 8 when employed in water remediation.

Despite of this, it is evident that the Fe incorporation improved the capability of Z for As adsorption. This issue has been previously reported in several works. Bilici Baskan and Pala (2011) reported that Fe^{3+} modified clinoptilolite showed a significant As sorption (9,2 µg/g) when compared with untreated clinoptilolite (1,5 µg/g). Likewise, Suazo-Hernández et al. (2019) reported that the amount of As(V) adsorbed at equilibrium for Z loaded with zero-valent iron was 47.30 mg/g, while for natural zeolite, the value reached was about 1,78 mg/g.

Arsenic removal was over 90% using M and MZ adsorbents. Figure 8a shows the percentage of As removal from groundwater sample, versus time by employing both materials. Rapid As removal is observed during the first minutes of assays, reaching the equilibrium zone at around 30 and 60 min for M and MZ, respectively. Increasing the assay's time does not improve the adsorption capacity. In both cases, after 60 min of contact, over 93% of total arsenic was removed. Considering that the As concentration in the analyzed sample before treatment was 200 µg L^{-1}, that implies a residual As concentration of 10 µg L^{-1}, which is in concordance with the limit value recommended by WHO (World Health Organization 2011).

The satisfactory As adsorption efficiency of MZ in a real water sample could be ascribed to the synergistic combination between the zeolite and the magnetic phase. The zeolite has a high affinity for cation sorption, which could eliminate from the aqueous matrix cationic species that may compete with As for the active sites of the adsorbent, while the magnetic component promotes Fe–As coordination linkages providing the surface with higher functionality. (Václavíková et al. 2009).

In fact, the mechanisms of As adsorption onto iron moieties have been studied and reported in the open literature and mainly involve electrostatic interactions and the formation of surface complexes between As species and iron oxides.

In particular, As^{5+} is known to form inner sphere surface complexes, while As^{3+} forms both inner and outer sphere surface complexes with Fe moieties (Goldberg et al. 2001; Liu et al. 2015; Manning et al. 1998; Zhang et al. 2010). Besides, some authors informed a complex redox transformation of adsorbed arsenic because of the role played by reactive Fe (Liu et al. 2015; Yan et al. 2012). Figure 9 shows

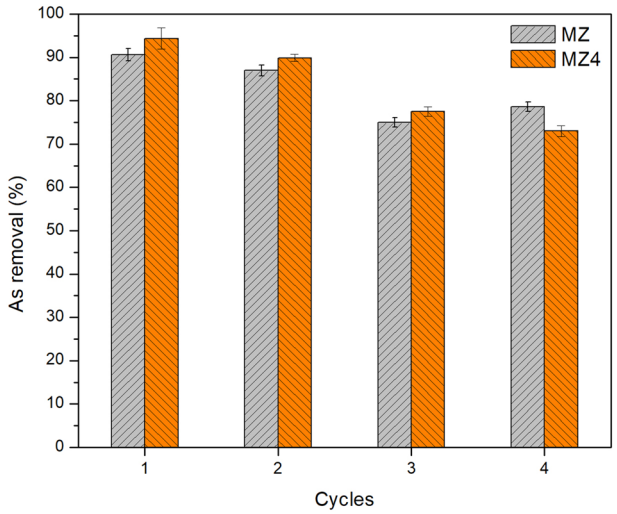

Fig. 10 Cycles of reuse of MZ and MZ4 for As adsorption in a real water sample

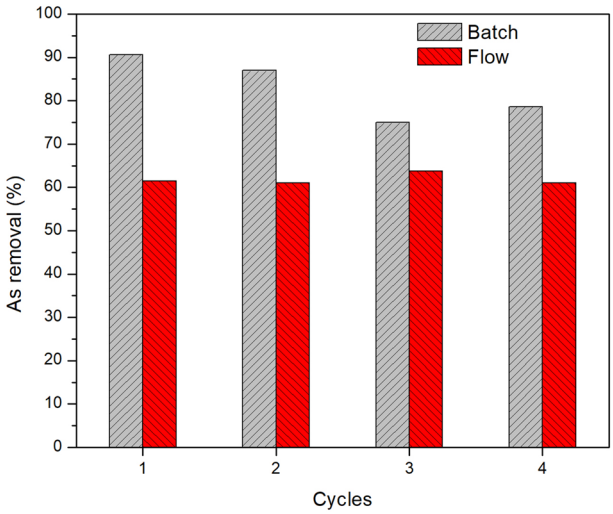

Fig. 11 Comparison between the efficiency of As removal in batch and flow procedures in repeated cycles

the different proposed mechanisms and the possible surface interaction between As and iron moieties within this work.

Reusability assays

From a practical implementation, the use of adsorbents for water decontamination highlights their possible reuse. In this sense, the reuse of an adsorbent not only reduces operating costs, but also the final amount of discarded material.

As shown in Fig. 10, there were no significant difference between the As removal of both magnetic composites. After the first adsorption cycle, MZ and MZ4 adsorbed 90% and 94% of total arsenic, respectively, reaching a residual As concentration lower to 10 µg L^{-1}. However, the adsorption capacity gradually decreases at 78 and 73% (40 µg L^{-1} As) for MZ and MZ4 materials throughout four cycles, respectively.

Stability assays

The stability of adsorbents in terms of leaching of their components into the treated water is undesirable. This is a critical property for evaluating the viability of adsorbent materials. In Argentina, the maximum iron concentration allowed in drinking water is 0.30 mg L^{-1} (CAA 2007).

Therefore, the amount of iron leached over the reuse cycles was evaluated for magnetic materials. In the framework of this contribution, it was evaluated during the reusability process of magnetic composites and raw magnetite. In the case of M, iron leaching was detected from the first cycles. After four consecutive adsorption cycles, the Fe concentration reached was 1.27 mg L^{-1}, which represents a value 4 times higher than the value allowed by legislation in Argentina (CAA, 2007). MZ and MZ4 composites did not exhibit iron leaching after four cycles. However, iron leaching was registered in both adsorbents after the fifth cycle, although the values registered were below the permissible limit. Similar trends were also previously informed in terms of the magnetite iron leaching compared with composite materials (Ai et al. 2011; Inbaraj et al. 2011; Liu et al. 2008). From these findings, it is evident that the formation of composites materials by incorporating magnetite phase into zeolite improves the stability of the proposed adsorbents, ensuring that they are suitable for practical implementation.

Flow assays

Industrial processes generally operate under continuous conditions. Therefore, the study of a continuous adsorption system provides a practical approach to applying of adsorbents in water treatment. The performance of the MZ composite for As adsorption was evaluated employing a continuous flow system. This composite was selected as a model based on the previous results.

For these assays, the mass adsorbent/water volume ratio was remained constant regarding batch assays. Therefore, a direct comparison of both assays may be possible. Figure 11 shows a comparison of the results obtained for the batch and flow assays.

The MZ composite shows a constant efficiency regarding As removal (%) throughout four consecutive adsorption cycles without iron leaching. Despite this, in flow assays, removal of As (61%) decreases regarding batch assays. The reduction in removal efficiency can be explained by taking into account that in flow tests, the contact time between the adsorbent and the sample is much lower than the equilibrium

time (Adrian Bonilla et al. 2015). In addition, the exposed surface area of the adsorbent packed in a column decrease concerning batch systems. In this regard, the compaction of the material in the column due to the flow and the formation of channels can affect the efficiency.

The efficiency of the continuous process could be improved using columns in series to optimize the adsorption process. In this way, the effluent from one column would be the feed for the next column.

Concluding remarks

The preparation of magnetic zeolite nanocomposites has been achieved by direct co-precipitation of magnetic nanoparticles. XRD analysis confirmed the presence of both crystalline patterns in the nanocomposites. The FTIR indicated that covalent interaction between zeolite and magnetite nanoparticles takes place. In addition, morphologic analysis revealed that the zeolite caused the stabilization of magnetite nanoparticles leading to smaller ones. Zeta potential data indicated that novel materials with different properties regarding the raw Z and M were obtained.

The performance of magnetic zeolite nanocomposites in removing As from groundwater was found to be better than the one corresponding to Z. Although M exhibited higher efficiency, it lacks stability in the media intended for its application. The removal efficiency of the proposed materials was compared with that of a material of similar composition (nZVI); however, the adsorption kinetics of these materials was found to be fluctuating with respect to time.

The assays aimed to evaluate the efficiency of the best adsorbent (MZ) in a flow system revealed that it falls concerning the batch assays. However, the removal percentage remained almost constant throughout the four cycles explored.

The system developed for As removing is economical, rapid, and capable of operating under natural conditions. Its implementation may be extended to other groundwater sources as well as to other types of water matrix, such as superficial or saline.

Acknowledgements The authors acknowledge the financial support of UNS, CONICET, and ANPCyT. Lic. V. N. Scheverin acknowledges CIC (Comisión de Investigaciones Científicas de la Provincia de Buenos Aires).

Funding This work was supported by CONICET, ANPCyT and UNS, Argentina.

Declarations

Conflict of interest We declare that there are not conflicts of interest between the authors.

References

Abdullah NH, Shameli K, Etesami M, Chan Abdullah E, Abdullah LC (2017) Facile and green preparation of magnetite/zeolite nanocomposites for energy application in a single-step procedure. J Alloy Compd 719:218–226. https://doi.org/10.1016/j.jallcom.2017.05.028

Abdullah NH, Shameli K, Abdullah EC, Abdullah LC (2019) Solid matrices for fabrication of magnetic iron oxide nanocomposites: Synthesis, properties, and application for the adsorption of heavy metal ions and dyes. Compos B Eng 162:538–568. https://doi.org/10.1016/j.compositesb.2018.12.075

Ai L, Zhang C, Liao F, Wang Y, Li M, Meng L, Jiang J (2011) Removal of methylene blue from aqueous solution with magnetite loaded multi-wall carbon nanotube: Kinetic, isotherm and mechanism analysis. J Hazard Mater 198:282–290. https://doi.org/10.1016/j.jhazmat.2011.10.041

Al Rawahi W (2016) Vanadium, Arsenic and Fluoride in Natural Waters from Argentina and Possible Impact on Human Health, Guildford; PhD Thesis; UK; University of Surrey 71–73

Alswata AA, Ahmad MB, Al-Hada NM, Kamari HM, Hussein MZ, Ibrahim NA (2017) Preparation of Zeolite/Zinc Oxide Nanocomposites for toxic metals removal from water. Results Phys 7:723–731. https://doi.org/10.1016/j.rinp.2017.01.036

Arruebo M, Fernández-Pacheco R, Irusta S, Arbiol J, Ibarra MR, Santamaría J (2006) Sustained release of doxorubicin from zeolite-magnetite nanocomposites prepared by mechanical activation. Nanotechnology 17(16):4057–4064. https://doi.org/10.1088/0957-4484/17/16/011

Auge M, Espinosa Viale G, Sierra L (2013) Arsénico en el agua subterránea de la Provincia de Buenos Aires. In: VIII Congreso Argentino de Hidrogeología: Aguas subterráneas recurso estratégico 2:58–63 https://doi.org/10.13140/RG.2.1.3333.4245

Azcona P, Zysler R, Lassalle V (2016) Simple and novel strategies to achieve shape and size control of magnetite nanoparticles intended for biomedical applications. Colloids Surf a: Physicochem Eng Asp 504:320–330. https://doi.org/10.1016/j.colsurfa.2016.05.064

Bakatula EN, Mosai AK, Tutu H (2015) Removal of uranium from aqueous solutions using ammonium-modified zeolite. South Afr J Chem 68:165–171. https://doi.org/10.17159/0379-4350/2015/v68a23

Bhowmick S, Chakraborty S, Mondal P, Van Renterghem W, Van den Berghe S, Roman-Ross G, Chatterjee D, Iglesias M (2014) Montmorillonite-supported nanoscale zero-valent iron for removal of arsenic from aqueous solution: Kinetics and mechanism. Chem Eng J 243:14–23. https://doi.org/10.1016/j.cej.2013.12.049

Bilici Baskan M, Pala A (2011) Removal of arsenic from drinking water using modified natural zeolite. Desalination 281:396–403. https://doi.org/10.1016/j.desal.2011.08.015

Blanco MDC, Paoloni JD, Morrás HJM, Fiorentino CE, Sequeira M (2006) Content and distribution of arsenic in soils, sediments and groundwater environments of the Southern Pampa Region. Argentina Environ Toxicol 21(6):561–574. https://doi.org/10.1002/tox.20219

Blanco Varela MT, Martínez Ramírez S, Ereña I, Gener M, Carmona P (2006) Characterization and pozzolanicity of zeolitic rocks from two Cuban deposits. Appl Clay Sci 33(2):149–159. https://doi.org/10.1016/J.CLAY.2006.04.006

Bonilla-Petriciolet A, Mendoza-Castillo DI, Reynel-Avila HE, Aguayo-Villareal I (2015) Perspectivas de la intensificación de procesos de adsorción empleando carbón activado para la remoción de contaminantes prioritarios del agua. Bol Grupo Español Carbón 36:17–21

Bosînceanu R, Suliţanu N (2008) Synthesis and characterization of FeO(OH)/Fe_3O_4 nanoparticles encapsulated in zeolite matrix. J Optoelecton Adv Mater 10(12):3482–3486

Bruce IJ, Taylor J, Todd M, Davies MJ, Borioni E, Sangregorio C, Sen T (2004) Synthesis, characterisation and application of silica-magnetite nanocomposites. J Magn Magn Mater 284:145–160. https://doi.org/10.1016/J.JMMM.2004.06.032

Bundschuh J, Litter MI, Parvez F, Román-Ross G, Nicolli HB, Jean JS, Liu CW, López D, Armienta MA, Guilherme LRG, Cuevas AG, Cornejo L, Cumbal L, Toujaguez R (2012) One century of arsenic exposure in Latin America: A review of history and occurrence from 14 countries. Sci Total Environ 429:2–35. https://doi.org/10.1016/J.SCITOTENV.2011.06.024

Bundschuh J, Pérez Carrera A, Litter MI (2008) Distribución del arsénico en las regiones ibérica e iberoamericana. Editorial Programa Iberoamericano de Ciencia y Tecnología Para El Desarrollo

Burris LE, Juenger MCG (2016) The effect of acid treatment on the reactivity of natural zeolites used as supplementary cementitious materials. Cemen Concr Res 79:185–193. https://doi.org/10.1016/j.cemconres.2015.08.007

CAA (2007) Código Alimentario Argentino. Capitulo XII. Bebidas Hídricas, Agua y Agua Gasificada. Artículo 982. Res Conj. SPRyRS y SAGPyA N° 68/2007 N° 196/2007. Ley 18284. Buenos Aires: Marzocchi

Chen X, Zeng XC, Wang J, Deng Y, Ma T, Guoji E, Mu Y, Yang Y, Li H, Wang Y (2017) Microbial communities involved in arsenic mobilization and release from the deep sediments into groundwater in Jianghan plain, Central China. Sci Total Environ 579:989–999. https://doi.org/10.1016/j.scitotenv.2016.11.024

Darminto Cholishoh MN, Perdana FA, Baqiya MA, Mashuri Cahyono Y (2011) Preparing Fe_3O_4 nanoparticles from Fe2+ ions source by co-precipitation process in various pH. AIP Confer Proc 10(1063/1):3667264

Dorathi PJ, Kandasamy P (2012) Dechlorination of chlorophenols by zero valent iron impregnated silica. J Environ Sci 24(4):765–773. https://doi.org/10.1016/S1001-0742(11)60817-6

Doula MK (2007) Synthesis of a clinoptilolite-Fe system with high Cu sorption capacity. Chemosphere 67(4):731–740. https://doi.org/10.1016/j.chemosphere.2006.10.072

Elizalde-Gonzalez MP, Mattusch J, Wennrich R (2001) Application of natural zeolites for preconcentration of arsenic species in water samples. J Environ Monit 3(1):22–26. https://doi.org/10.1039/b006636m

Garelick H, Dybowska A, Valsami-Jones E, Priest ND (2005) Remediation technologies for arsenic contaminated drinking waters. J Soils Sediments 5(3):182–190. https://doi.org/10.1065/jss2005.06.140

Gil-Llambias FJ, Escudey-Castro AM (1982) Use of zero point charge measurements in determining the apparent surface coverage of molybdena in MoO3/γ-Al2O3 catalysts. J Chem Soc Chem Commun. https://doi.org/10.1039/C39820000478

Gnanaprakash G, Mahadevan S, Jayakumar T, Kalyanasundaram P, Philip J, Raj B (2007) Effect of initial pH and temperature of iron salt solutions on formation of magnetite nanoparticles. Mater Chem Phys 103(1):168–175. https://doi.org/10.1016/j.matchemphys.2007.02.011

Goldberg S, Johnston CT (2001) Mechanisms of arsenic adsorption on amorphous oxides evaluated using macroscopic measurements, vibrational spectroscopy, and surface complexation modeling. J Colloid Interf Sci 234(1):204–216. https://doi.org/10.1006/jcis.2000.7295

Gomez ML, Blarasin MT, Martínez DE (2009) Arsenic and fluoride in a loess aquifer in the central area of Argentina. Environ Geol 57(1):143–155. https://doi.org/10.1007/s00254-008-1290-4

Habuda-Stanić M, Ravančić M, Flanagan A (2014) A review on adsorption of fluoride from aqueous solution. Materials 7(9):6317–6366. https://doi.org/10.3390/ma7096317

Hao L, Liu M, Wang N, Li G (2018) A critical review on arsenic removal from water using iron-based adsorbents. RSC Adv 8(69):39545–39560. https://doi.org/10.1039/c8ra08512a

Horst MF, Alvarez M, Lassalle VL (2016) Removal of heavy metals from wastewater using magnetic nanocomposites: analysis of the experimental conditions. Separ Sci Technol 51(3):550–563. https://doi.org/10.1080/01496395.2015.1086801

Horst MF, Coral DF, Fernández van Raap MB, Alvarez M, Lassalle V (2017) Hybrid nanomaterials based on gum Arabic and magnetite for hyperthermia treatments. Mater Sci Eng C 74:443–450. https://doi.org/10.1016/j.msec.2016.12.035

Inbaraj SB, Chen BH (2011) Dye adsorption characteristics of magnetite nanoparticles coated with a biopolymer poly(γ-glutamic acid). Bioresource Technol 102(19):8868–8876. https://doi.org/10.1016/j.biortech.2011.06.079

Jain N, Dwivedi MK, Agarwal R, Sharma P (2015) Removal of malachite green from aqueous solution by zeolite- iron oxide magnetic nanocomposite. J Envi Sci Toxicol Food Technol 9(6):2319–2399. https://doi.org/10.9790/2402-09614250

Kanel SR, Manning B, Charlet L, Choi H (2005) Removal of arsenic(III) from groundwater by nanoscale zero-valent iron. Environ Sci Technol 39(5):1291–1298. https://doi.org/10.1021/es048991u

Kanel SR, Greneche JM, Choi H (2006) Arsenic(V) removal from groundwater using nano scale zero-valent iron as a colloidal reactive barrier material. Environ Sci Technol 40(6):2045–2050. https://doi.org/10.1021/es0520924

Kharissova OV, Dias HVR, Kharisov BI (2015) Magnetic adsorbents based on micro- and nano-structured materials. RSC Adv 5(9):6695–6719. https://doi.org/10.1039/c4ra11423j

Kim W, Suh CY, Cho SW, Roh KM, Kwon H, Song K, Shon IJ (2012) A new method for the identification and quantification of magnetite-maghemite mixture using conventional X-ray diffraction technique. Talanta 94:348–352. https://doi.org/10.1016/j.talanta.2012.03.001

Korkuna O, Leboda R, Skubiszewska-Zięba J, Vrublevs'ka T, Gun'ko VM, Ryczkowski J, (2006) Structural and physicochemical properties of natural zeolites: Clinoptilolite and mordenite. Micropor Mesopor Mater 7(3):243–254. https://doi.org/10.1016/j.micromeso.2005.08.002

Kosmulski M (2016) Isoelectric points and points of zero charge of metal (hydr) oxides: 50 years after Parks' review. Adv Colloid Interf Sci 238:1–61. https://doi.org/10.1016/j.cis.2016.10.005

Lassalle VL, Zysler RD, Ferreira ML (2011) Novel and facile synthesis of magnetic composites by a modified co-precipitation method. Mater Chem Phys 130(1–2):624–634. https://doi.org/10.1016/j.matchemphys.2011.07.035

Lata S, Samadder SR (2016) Removal of arsenic from water using nano adsorbents and challenges: A review. J Environ Manag 166:387–406. https://doi.org/10.1016/j.jenvman.2015.10.039

Li Z, Beachner R, McManama Z, Hanlie H (2007) Sorption of arsenic by surfactant-modified zeolite and kaolinite. Micropor Mesopor Mater 105(3):291–297. https://doi.org/10.1016/j.micromeso.2007.03.038

Li Z, Wang L, Meng J, Liu X, Xu J, Wang F, Brookes P (2018) Zeolite-supported nanoscale zero-valent iron: New findings on simultaneous adsorption of Cd(II), Pb(II), and As(III) in aqueous solution and soil. J Hazard Mater 344:1–11. https://doi.org/10.1016/j.jhazmat.2017.09.036

Litter MI, Morgada ME, Bundschuh J (2010) Possible treatments for arsenic removal in Latin American waters for human consumption. Environ Pollut 158(5):1105–1118. https://doi.org/10.1016/J.ENVPOL.2010.01.028

Liu JF, Zhao ZS, Jiang GB (2008) Coating Fe_3O_4 magnetic nanoparticles with humic acid for high efficient removal of heavy metals in water. Environ Sci Technol 42(18):6949–6954. https://doi.org/10.1021/es800924c

Liu CH, Chuang YH, Chen TY, Tian Y, Li H, Wang MK, Zhang W (2015) Mechanism of arsenic adsorption on magnetite nanoparticles from water: thermodynamic and spectroscopic studies. Environ Sci Technol 49(13):7726–7734. https://doi.org/10.1021/acs.est.5b00381

Maity D, Agrawal DC (2007) Synthesis of iron oxide nanoparticles under oxidizing environment and their stabilization in aqueous and non-aqueous media. J Magn Magn Mater 308(1):46–55. https://doi.org/10.1016/j.jmmm.2006.05.001

Manning BA, Fendorf SE, Goldberg S (1998) Surface structures and stability of arsenic(III) on goethite: Spectroscopic evidence for inner-sphere complexes. Environ Sci Technol 32(16):2383–2388. https://doi.org/10.1021/es9802201

Matei E, Predescu C, Berbecaru A, Predescu A, TruşCĂa R (2011) Leaching tests for synthesized magnetite nanoparticles used as adsorbent for metal ions from liquid solutions. Dig J Nanomater Bios 6(4):1701–1708

Merola RB, Kravchenko J, Rango T, Vengosh A (2014) Arsenic exposure of rural populations from the Rift Valley of Ethiopia as monitored by keratin in toenails. J Expo Sci Environ Epidemiol 24(2):121–126. https://doi.org/10.1038/jes.2013.77

Mohammed R, El-Maghrabi HH, Younes AA, Farag AB, Mikhail S, Riad M (2017) SDS-goethite adsorbent material preparation, structural characterization and the kinetics of the manganese adsorption. J Mol Liq 231:499–508. https://doi.org/10.1016/J.MOLLIQ.2017.02.041

Mthombeni NH, Mbakop S, Ochieng A, Onyango MS (2016) Vanadium (V) adsorption isotherms and kinetics using polypyrrole coated magnetized natural zeolite. J Taiwan Inst Chem Eng 66:172–180. https://doi.org/10.1016/j.jtice.2016.06.016

Nasrazadani S, Raman A (1993) The application of infrared spectroscopy to the study of rust systems—II. Study of cation deficiency in magnetite (Fe_3O_4) produced during its transformation to maghemite (γ-Fe_2O_3) and hematite (α-Fe_2O_3). Corros Sci 34(8):1355–1365. https://doi.org/10.1016/0010-938X(93)90092-U

Nicolás P, Saleta M, Troiani H, Zysler R, Lassalle V, Ferreira ML (2013) Preparation of iron oxide nanoparticles stabilized with biomolecules: Experimental and mechanistic issues. Acta Biomater 9(1):4754–4762. https://doi.org/10.1016/j.actbio.2012.09.040

Nordstrom DK (2002) Worldwide occurrences of arsenic in ground water. Science 296(5576):2143–2145. https://doi.org/10.1126/science.1072375

Olad A, Naseri B (2010) Preparation, characterization and anticorrosive properties of a novel polyaniline/clinoptilolite nanocomposite. Prog Org Coat 67(3):233–238. https://doi.org/10.1016/J.PORGCOAT.2009.12.003

Paoloni JD, Sequeira ME, Espósito ME, Fiorentino CE, Blanco MDC (2009) Arsenic in water resources of the southern pampa Plains, Argentina. J Environ Pub Health. https://doi.org/10.1155/2009/216470

Parks GA (1967) Aqueous surface chemistry of oxides and complex oxide minerals: Isoelectric point and zero point of charge. Amer Chem Soc Adv Chem Ser 67:121–160

Pizarro C, Rubio MA, Escudey M, Albornoz MF, Muñoz D, Denardin J, Fabris JD (2015) Nanomagnetite-zeolite composites in the removal of arsenate from aqueous systems. J Braz Chem Soc 26(9):1887–1896. https://doi.org/10.5935/0103-5053.20150166

Popescu RC, Andronescu E, Vasile BS (2019) Recent advances in magnetite nanoparticle functionalization for nanomedicine. Nanomaterials 9(12):1–31. https://doi.org/10.3390/nano9121791

Rahmani F, Haghighi M, Amini M (2015) The beneficial utilization of natural zeolite in preparation of Cr/clinoptilolite nanocatalyst used in CO2-oxidative dehydrogenation of ethane to ethylene. J Ind Eng Chem 31:142–155. https://doi.org/10.1016/J.JIEC.2015.06.018

Rango T, Vengosh A, Dwyer G, Bianchini G (2013) Mobilization of arsenic and other naturally occurring contaminants in groundwater of the Main Ethiopian Rift aquifers. Water Res 47(15):5801–5818. https://doi.org/10.1016/j.watres.2013.07.002

Russo V, Toriggia LF, Jacobo SE (2014) Natural clinoptilolite – zeolite loaded with iron for aromatic hydrocarbons removal from aqueous solutions. J Mater Sci 49:614–620. https://doi.org/10.1007/s10853-013-7741-7

Salem Attia TM, Hu XL, Yin DQ (2014) Synthesised magnetic nanoparticles coated zeolite (MNCZ) for the removal of arsenic (As) from aqueous solution. J Exp Nanosci 9(6):551–560. https://doi.org/10.1080/17458080.2012.677549

Singh LH, Pati SS, Coaquira JAH, Matilla J, Guimarães EM, Oliveira AC, Kuzmann E, Garg VK (2016) Magnetic interactions in cubic iron oxide magnetic nanoparticle bound to zeolite. J Magn Magn Mater 416:98–102. https://doi.org/10.1016/j.jmmm.2016.05.003

Smedley PL, Kinniburgh DG (2002) A review of the source, behaviour and distribution of arsenic in natural waters. Appl Geochem 17(5):517–568. https://doi.org/10.1016/S0883-2927(02)00018-5

Smedley PL, Nicolli HB, Macdonald DMJ, Barros AJ, Tullio JO (2002) Hydrogeochemistry of arsenic and other inorganic constituents in groundwaters from La Pampa, Argentina. Appl Geochem 17(3):259–284. https://doi.org/10.1016/S0883-2927(01)00082-8

Stoia M, Istratie R, Păcurariu C (2016) Investigation of magnetite nanoparticles stability in air by thermal analysis and FTIR spectroscopy. J Therm Anal Calorim 125(3):1185–1198. https://doi.org/10.1007/s10973-016-5393-y

Suazo-Hernández J, Sepúlveda P, Manquián-Cerda K, Ramírez-Tagle R, Rubio MA, Bolan N, Sarkar B, Arancibia-Miranda N (2019) Synthesis and characterization of zeolite-based composites functionalized with nanoscale zero-valent iron for removing arsenic in the presence of selenium from water. J Hazard Mater 373:810–819. https://doi.org/10.1016/j.jhazmat.2019.03.125

Sun ZX, Su FW, Forsling W, Samskog PO (1998) Surface characteristics of magnetite in aqueous suspension. J Colloid Interface Sci 197(1):151–159. https://doi.org/10.1006/jcis.1997.5239

Tanboonchuy V, Grisdanurak N, Liao CH (2012) Background species effect on aqueous arsenic removal by nano zero-valent iron using fractional factorial design. J Hazard Mater. https://doi.org/10.1016/j.jhazmat.2011.11.090

Václavíková M, Stefusova K, Ivaničová L, Jakabsky S, Gallios GP (2009) Magnetic Zeolite as Arsenic Sorbent, 51–59. In: Václavíková M, Vitale K, Gallios GP, Ivaničová L (eds.) Water Treatment Technologies for the Removal of High-Toxicity Pollutants. NATO Science for Peace and Security Series C: Environmental Security. Springer, Dordrecht. https://doi.org/10.1007/978-90-481-3497-7_5

Villaamil Lepori EC (2015) Hidroarsenicismo crónico regional endémico en Argentina. Acta Bioquimica Clinica Latinoamericana 49(1):83–104

Wang W, Zhou M, Mao Q, Yue J, Wang X (2010) Novel NaY zeolite-supported nanoscale zero-valent iron as an efficient heterogeneous Fenton catalyst. Catal Commun 11(11):937–941. https://doi.org/10.1016/j.catcom.2010.04.004

World Health Organization (2011) Guidelines for drinking-water quality. World Health Organization

Yamaura M, Fungaro DA (2013) Synthesis and characterization of magnetic adsorbent prepared by magnetite nanoparticles and zeolite from coal fly ash. J Mater Sci 48(14):5093–5101. https://doi.org/10.1007/s10853-013-7297-6

Yan W, Ramos MAV, Koel BE, Zhang WX (2012) As(III) sequestration by iron nanoparticles: Study of solid-phase redox transformations with X-ray photoelectron spectroscopy. J Phy Chem C 116(9):5303–5311. https://doi.org/10.1021/jp208600n

Yuan ML, Song C, Yan GJ (2011) Some research on the magnetic X zeolite composites. Adv Mater Res 311–313:2040–2047. https://doi.org/10.4028/www.scientific.net/AMR.311-313.2040

Zhang S, Li X, Chen JP (2010) An XPS study for mechanisms of arsenate adsorption onto a magnetite-doped activated carbon fiber. J Colloid Interface Sci 343(1):232–238. https://doi.org/10.1016/J.JCIS.2009.11.001